Artificial Enzymes

International Edition: DOI: 10.1002/anie.201802946
German Edition: DOI: 10.1002/ange.201802946

An Artificial Heme Enzyme for Cyclopropanation Reactions

*Lara Villarino, Kathryn E. Splan, Eswar Reddem, Lur Alonso-Cotchico, Cora Gutiérrez de Souza, Agustí Lledós, Jean-Didier Maréchal, Andy-Mark W. H. Thunnissen, and Gerard Roelfes**

Abstract: *An artificial heme enzyme was created through self-assembly from hemin and the lactococcal multidrug resistance regulator (LmrR). The crystal structure shows the heme bound inside the hydrophobic pore of the protein, where it appears inaccessible for substrates. However, good catalytic activity and moderate enantioselectivity was observed in an abiological cyclopropanation reaction. We propose that the dynamic nature of the structure of the LmrR protein is key to the observed activity. This was supported by molecular dynamics simulations, which showed transient formation of opened conformations that allow the binding of substrates and the formation of pre-catalytic structures.*

Engineered heme proteins such as cytochrome P450 enzymes, myoglobin, and cyctochrome C have emerged as excellent catalysts for new-to-nature reactions,[1,2] including carbene-transfer reactions such as cyclopropanations,[3–7] olefinations, and[8,9] N–H,[10,11] Si–H,[12] and B–H insertion reactions.[13] These enzymes have proven amenable to optimization by both genetic methods and co-factor replacement.[14–20] A common feature of these (designed) heme enzymes is that they contain a large hydrophobic substrate binding pocket orthogonal to the plane of the heme moiety. Alternatively, significant effort has been devoted to the de novo design of heme proteins, particularly based on 4-helix bundles,[21–25] antibodies, or other proteins,[26,27] yet none of these has found application in catalysis of new-to-nature reactions. A key difference is that these artificial heme enzymes generally do not present a defined binding site suitable for binding the often hydrophobic substrates. Here, we report a novel artificial heme enzyme based on the lactococcal multidrug resistance regulator (LmrR), which is capable of catalyzing abiological enantioselective cyclopropanation reactions. Moreover, we propose that the structural dynamics of the artificial heme enzyme are key to its catalytic activity.

LmrR is a homodimeric protein with a unique and highly dynamic structure that is key to its biological function.[28,29] It presents an unusually large hydrophobic and promiscuous binding pocket at the dimer interface, which has proven to be very suitable for the creation of a novel active site through anchoring of a catalytically active Cu^{II} complex inside. The resulting artificial metalloenzymes have been applied successfully in enantioselective Lewis acid catalysis.[30–33] In particular, supramolecular assembly of the artificial metalloenzyme through combination with a Cu^{II}-phenanthroline complex proved powerful, giving rise to excellent enantioselectivity in the Friedel–Crafts alkylation reaction.[34] The diversity of reactions catalyzed by LmrR-based artificial enzymes led us to believe that the LmrR scaffold could be extended to other catalyst types, including heme-based catalysts.

The design was based on an LmrR variant that includes a C-terminal strep-tag and has two mutations in the DNA binding domain (K55D and K59Q), which facilitates expression and purification.[31] A second mutant, LmrR_W96A, was prepared to assess the effect of the tryptophan residues in the hydrophobic pore (W96 and W96′, with the prime denoting the dimer related subunit), which are known to play a role in the binding of guest molecules.[28]

The artificial heme enzymes were created through self-assembly by adding iron (III) chloroprotoporphyrin IX (Hemin) to the corresponding protein LmrR variant in a buffered solution (50 mM $KHPO_4$, 150 mM NaCl, pH 7; Scheme 1). The interaction of hemin with LmrR was examined by electronic absorption spectroscopy. The visible spectrum of hemin at pH 7.0 (Figure 1a) exhibits a broad Soret band and a weak peak around 610 nm in the Q band region, which is characteristic of a π–π porphyrin dimer that was previously shown to predominate in aqueous hemin solutions at neutral pH.[35,36] Addition of LmrR caused a substantial sharpening in the Soret and Q-band regions, resulting in a spectrum that is similar to that of hemin in organic solvents.[36] Clearly, upon addition of the protein, the dimeric porphyrin structure is disrupted and the hemin is in

[*] Dr. L. Villarino, Dr. E. Reddem, M. Sc. C. Gutiérrez de Souza, Prof. G. Roelfes
Stratingh Institute for Chemistry, University of Groningen
Nijenborgh 4, 9747 AG Groningen (The Netherlands)
E-mail: j.g.roelfes@rug.nl
Prof. K. E. Splan
Department of Chemistry, Macalester College
1600 Grand Avenue, Saint Paul, MN 55105 (USA)
M. Sc. L. Alonso-Cotchico, Prof. A. Lledós, Prof. J. D. Maréchal
Departament de Química, Universitat Autònoma de Barcelona
Edifici C.n., 08193 Cerdanyola del Vallés, Barcelona (Spain)
Dr. A. M. W. H. Thunnissen
Groningen Biomolecular Sciences and Biotechnology Institute
University of Groningen
Nijenborgh 4, 9747 AG Groningen (The Netherlands)
Supporting information and the ORCID identification number(s) for the author(s) of this article can be found under: https://doi.org/10.1002/anie.201802946.

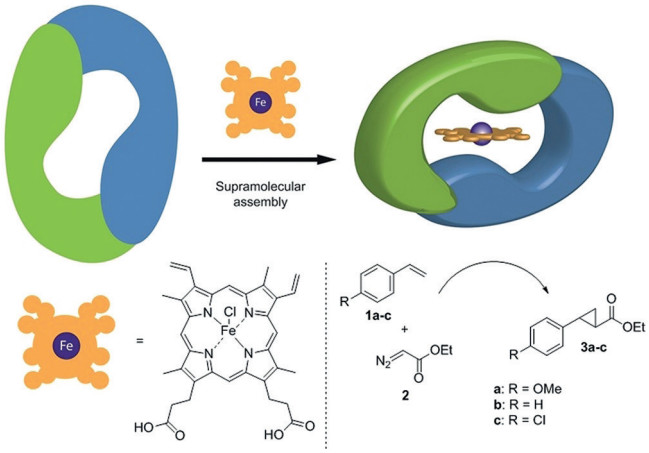

Scheme 1. Schematic representation of the assembly of the LmrR-based artificial heme enzyme and the catalyzed enantioselective cyclopropanation reaction.

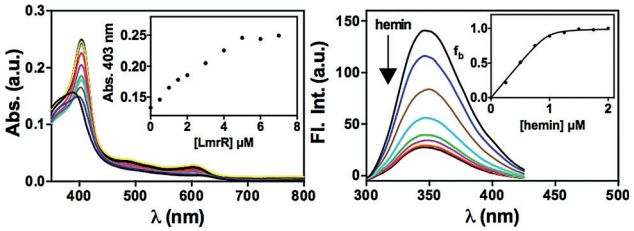

Figure 1. a) Electronic absorption spectra upon the addition of LmrR to 5 μM hemin. Inset: Changes in absorption values as a function of protein concentration. Buffer: 50 mM phosphate buffer/150 mM NaCl, pH 7.0. b) Fluorescence spectra upon the addition of hemin to 1 μM LmrR dimer. Inset: Fraction of LmrR bound to hemin as a function of added hemin concentration. Buffer: 50 mM phosphate buffer/150 mM NaCl, pH 7.0.

a monomeric form. Monitoring spectral changes as a function of added protein indicates that hemin binds to LmrR with a ratio of one hemin per dimeric protein. This stoichiometry was further confirmed by monitoring tryptophan fluorescence quenching, which was complete upon the addition of 1 equivalent of hemin per LmrR dimer (Figure 1b). Fitting of fluorescence titration data yields a dissociation constant (K_D) of 38 ± 27 nM, thus indicating that the affinity of the protein for hemin is quite high, and is in fact comparable to or stronger than previously measured for other flat, planar molecules.[28]

In contrast, UV/vis titration of hemin with LmrR_W96A results in a loss of spectral intensity, but no substantial change in spectral line shape, likely owing to non-specific binding on the protein surface (Figure S4). These results clearly show that W96/W96′ play a key role in the interaction of hemin with LmrR, leading to a monomeric hemin structure, and indicate that hemin lies either partly or entirely within the hydrophobic pocket.

The Hemin/LmrR stoichiometry and the importance of W96/W96′ in complex formation are further supported by the crystal structure of LmrR co-crystallized with hemin (Figure 2 and Figure S6). Crystals diffracting to sufficiently high resolution could be obtained only for an LmrR that had the

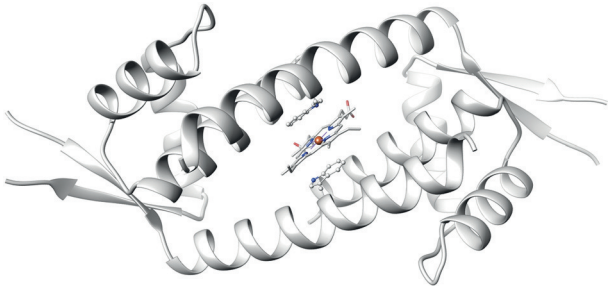

Figure 2. Crystal structure of LmrR⊂heme (PDB ID: 6FUU). The protein crystallized in a tetragonal crystal form with one polypeptide chain occupying the asymmetric unit; the functional dimer (here shown in cartoon representation) is formed by a crystallographic dyad. In the electron density maps, the polypeptide chain is well defined, except for the tip region of the β-wing (residues 70–73) and the N- and C-termini (residues 1–4 and 109–131, including the C-terminal strep-tag). These regions show a high degree of disorder and were excluded from the final model. The heme is stacked in between the side chains of W96/W96′ (for clarity only one of the alternate heme binding orientations is shown).

K55 and K59 residues reintroduced. The overall conformation of LmrR is similar to that observed in previously published drug-bound complexes.[28] Electron density in between the indole rings of the central W96/W96′ pair is attributed to the presence of the bound heme. Clear density is observed only for the porphyrin ring, owing in part to a crystallographic 2-fold axis, but also to a lack of specific stabilizing interactions with the polar peripheral heme substituents. The heme, lacking the axial chloride ligand, was modelled in the LmrR crystal structure with four alternate binding modes, differing by rotations around a central axis perpendicular to the plane of the heme, and by a flip of the heme due the crystallographic 2-fold symmetry (Figure S6). In all binding modes, the heme iron is shielded at either side of the heme by the indole ring of W96 and W96′ and lies at an average distance of around 4 Å from the carbon atoms, thus suggesting cation–π interactions. Further stabilization is provided by van der Waals contacts with hydrophobic residues in the vicinity of the central tryptophan pair, namely, M8, A11, and V15 (and their equivalents from the dimer mate). This structure is unlikely to allow catalysis since the catalytic iron is fully shielded and cannot be accessed by substrates. However, the crystal structure already suggests considerable dynamics in the binding of the heme, which may include catalytically viable conformations. This was supported by molecular dynamics (MD) simulations (see below).

The potential of the artificial heme enzymes in catalysis was examined in the cyclopropanation of *o*-methoxystyrene (**1a**) with ethyldiazoacetate (EDA, **2**) under anaerobic conditions as the benchmark reaction (Table 1 and Table S4). In the absence of LmrR, the reaction was sluggish, and diethyl fumarate (**4**), which results from the dimerization of EDA, was found as the major product (entry 1). The artificial heme enzyme (LmrR⊂heme) was assembled in situ by adding 1 mol% of hemin to a slight excess (1.1 equiv) of LmrR in previously deoxygenated 50 mM KPi buffer pH 8.0. The LmrR⊂heme-catalyzed reaction requires addition of

Table 1: Results of cyclopropanation reaction of styrene derivatives **1a–c** with EDA (**2**) catalyzed by LmrR⊂heme.[a]

entry	LmrR	**1**[c]	**3**	Yield [%]	TTN	3/4	*ee* [%][b]
1	–	**1a**	**3a**	5±2	51	0.8	–
2	LmrR	**1a**	**3a**	25±11	247	11	17±5
3	LmrR_F93A	**1a**	**3a**	23±2	232	9	11±1
4	LmrR_D100A	**1a**	**3a**	38±8	375	20	24±5
5	LmrR_W96A	**1a**	**3a**	28±13	276	8	<5
6	LmrR_V15A	**1a**	**3a**	1.5±0.5	15	3	17±1
7	LmrR_M8A	**1a**	**3a**	36±13	359	15	44±12
8[c]	LmrR_M8A	**1a**	**3a**	45±9	449	6	51±14
9[c]	–	**1b**	**3b**	6±0	59	n.d	–
10[c]	LmrR_M8A	**1b**	**3b**	39±13	391	n.d	38±5[d]
11[c]	–	**1c**	**3c**	1±0	12	0.2	–
12[c]	LmrR_M8A	**1c**	**3c**	35±13	351	3	25±5

[a] Conditions: 1 (30 mM), 2 (10 mM), hemin (1 mol%; 10 μM), LmrR_X (1.1 mol%; 11 μM) in 50 mM phosphate buffer (pH 8.0), under Ar, at 4 °C for 18 h; Results are the average of at least two independent experiments, both carried out in duplicate. [b] *ee* of the *trans* product; *trans*/*cis* > 85:15. [c] pH 7.0. [d] *ee* of the 1*R*, 2*R* enantiomer.[37]

sodium dithionate as a reductant to generate the Fe^{II} heme, which is the active complex required for carbene generation. The reaction was started by adding 30 mM of **1a** and 10 mM of **2**. After 18 h at 4 °C, the *trans* isomer of the cyclopropanation product **3a** (*trans*/*cis* = 92:8) was obtained as the major product in 25% yield, which corresponds to a total turnover number (TTN) of 247, and with an *ee* of 17%. (entry 2). The only detectable side product was diethyl fumarate (**4**), with 28 turnovers. These results clearly show the acceleration and chemoselectivity due to the LmrR scaffold compared to the reactions catalyzed by hemin alone under the same conditions.

The role of the protein scaffold was explored further by mutagenesis of residues in and around the hydrophobic pore. In addition to W96 (see above), residues M8, V15, F93, and D100 were mutated to alanine (see the Supporting Information). With the exception of V15A, all mutants showed significant protein enhanced catalytic activity that was comparable or greater than LmrR itself (entry 3–7). Surprisingly, this was also the case for LmrR_W96A, albeit with a complete loss of enantioselectivity. We attribute this to hemin–LmrR_W96A association away from the hydrophobic pore, which may result in assemblies that are catalytically active but lack the defined chiral interactions to induce enantioselectivity. A significant increase in activity was observed in case of the mutants D100A and M8A, with the latter also giving rise to the highest enantioselectivity of 44% *ee* (entry 7).

Further optimization of the reactions conditions was performed with this mutant (Tables S5,6). It was found that a threefold excess of styrene over EDA and pH 7.0 gave the optimal conditions in terms of activity and selectivity (entry 8).

The activity of LmrR_M8A⊂heme was compared for substrates **1a–c**. (entries 8–12). In all cases, the artificial heme enzyme significantly outperformed the free hemin cofactor. The enantioselectivity observed ranged from 25% *ee* in the case of **3c** (entry 12) to 51% *ee* in the case of **3a** (entry 8).

The observed catalytic activity and enantioselectivity are difficult to rationalize based on the crystal structure, which shows the catalytic iron center sandwiched between the two tryptophan residues, where it is inaccessible for the substrates. To gain more insight into the origin of the catalytic activity, computational studies were performed.

Calculations were focused on determining the conformational rearrangement required for LmrR⊂heme to allow substrate binding and the reaction to take place. Local and global rearrangements of the protein were assessed for the binding of the heme as well as in presence of the substrates by combining protein–ligand docking, quantum mechanics calculations, and large-scale molecular dynamics simulations.

Protein–ligand dockings of both the heme (**5**) and its adduct with the carbene intermediate (**6**; Figure S6) were carried out on LmrR, starting from the LmrR⊂heme crystal structure. Local rearrangements were assessed by introducing rotameric flexibility for all the amino acids at the dimer interface. For **5** and **6,** four binding poses with good predicted affinity (ChemScore values higher than 50 units) were found for both cases (Table S3). They correspond to different orientations of the heme group as a result of rotations around the axis perpendicular to the average plane of the heme passing through the metal. The best docking solutions of LmrR⊂**5** show the heme sandwiched between W96/W96′, similar to the crystal structure. However, in the case of the carbene complex (LmrR⊂**6**), some low-energy solutions present W96′ rotated towards the solvent, thus providing space to accommodate the co-substrate (Figure S1 in the Supporting Information). To assess the structural rearrangement of LmrR upon heme binding, the four predicted structures of LmrR⊂**5** and LmrR⊂**6** were submitted to 100 ns MD simulations.

Cluster analysis shows high stability for the LmrR⊂heme complex (Figure S8), with W96 and W96′ generating a hydrophobic patch that sandwiches the heme. Some of the most populated clusters of the LmrR⊂**5** system (clusters 1 and 3–6) show high similarity with the crystal structure, with the iron atom inaccessible to solvent (Figure 3a). On the other hand, clusters 0 and 2 (see the Supporting Information for details) show changes in the orientation of the α helix containing W96′ (α4) and a flip of the W96′ indole towards the outside of the pore (Figure 3b and Figure S10). These predicted conformational changes are in agreement with previous reports in which it was suggested that flexibility in the orientation of α4 is a major contributor to the ability of LmrR to structurally adapt to different drug molecules.[29] These changes in the protein structure are accompanied by a significant displacement of the heme towards the solvent. The result is an opened conformation that has significant free space on the axial face of the heme group. This appears to be of key importance to catalysis, since the iron site becomes accessible to bind the carbene, which allows the reaction occur.

MD simulations of the LmrR⊂heme–carbene complex (LmrR⊂**6**) show that this opened conformation is indeed capable of accommodating the carbene moiety. The simulations further underline the importance of W96′ in controlling the accessibility of the heme–carbene complex. With W96′ pointing towards the hydrophobic core, the heme–carbene is directed towards the solvent, where it will be accessible for the styrene co-substrate (Figure 3c). Rotation of W96′ to the

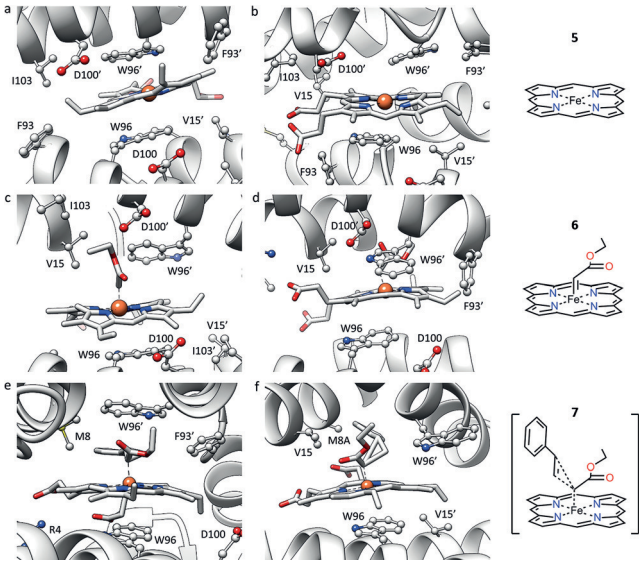

Figure 3. Representative structures resulting from MD simulations. a, b) The LmrR-heme system (cluster 3, RMSD with crystal 1.634 Å (a) and cluster 2 RMSD with crystal 2.471 Å (b); 400 ns MD simulation). c, d) The LmrR–heme–carbene system (cluster 0, RMSD with crystal of 0.548 Å (c) and cluster 2, RMSD with crystal of 1.000 Å (d); 400 ns MD simulation). e, f) The cyclopropanation transition state (with LmrR (e) and with LmrR_M8A (f); 100 ns MD simulation).

outside of the pore causes the heme–carbene (**6**) to remain at the dimer interface (Figure 3d, S8).

Finally, the effect of the second substrate (styrene) was studied. First, the transition-state (TS) geometry that leads to the generation of the 1*R*,2*R* cyclopropane was obtained by QM calculations (Figure S7) and then subjected to the same analysis as before (Table S3). The majority of the structures (clusters 0, 2 and 3) correspond to LmrR with a broader dimer interface where the two helices containing the W96/W96′ residues appear further separated and are thus capable of accommodating the catalytic complex (Figure 3e). W96′ appears to be involved in stabilizing the TS structure through π stacking with the phenyl group of the styrene.

Since the M8A mutant showed the best results in catalysis, the dynamic behavior of this artificial metalloenzyme was also studied. For consistency, all the simulations were carried out under the same conditions as before. The system resulting from the docking of the heme linked to the TS structure for the 1*R*,2*R* enantiomeric product into the LmrR protein was selected as a starting point for a 100 ns MD simulation, which suggests that the effect of this mutation is mainly steric: the aromatic moiety of the styrene now occupies the free space resulting from the change of the large methionine into the much smaller alanine. Additionally, W96′ is flipped towards the solvent and thus contributes to binding of the TS structure into the dimer interface (Figure 3f).

The combined results demonstrate unequivocally that the cyclopropanation reaction occurs in the hydrophobic pocket of LmrR. Initially, this is counterintuitive: heme enzymes such as P450 enzymes usually present a large hydrophobic cavity for binding substrates whereas, in contrast, upon binding of hemin, the pocket of LmrR is fully occupied. However, the artificial enzyme exhibits good activity and shows enantioselectivity in catalysis. This is attributed to the dynamic nature of the LmrR-based artificial heme enzyme, involving substantial geometric rearrangement of the heme environment to allow binding of the substrates and their interaction with the heme. Indeed, the MD simulations show that the LmrR⊂heme complex undergoes significant conformational changes, giving rise to transient open conformations that make it possible to reach a pre-catalytic state, thereby allowing the reaction to proceed.

In conclusion, we have created an artificial heme enzyme based on the protein LmrR, which shows good activity and moderate enantioselectivity in an abiological reaction, that is, the catalytic cyclopropanation of styrenes. This is the first example of organometallic catalysis with an LmrR-based artificial metalloenzyme and thus illustrates the versatility of LmrR as a scaffold for artificial metalloenzymes design. A key finding is that the enzyme is active despite the fact that the crystal structure shows a tightly bound heme that appears inaccessible to substrates. It is proposed that the artificial enzyme can open up to allow formation of precatalytic structures as a result of a dynamic protein–heme assembly. Molecular dynamics studies add support to this hypothesis. This work suggests that dynamics have to be taken into account in the design of artificial enzymes and may be key to achieving catalytic activity.

Acknowledgements

The authors thank Dr. I. Drienovská and S. Chordia for help and advice on molecular biology, the European Synchrotron Radiation Facility (ESRF) for provision of synchrotron radiation facilities, and the beam-line staff of MASSIF-3 for their assistance. Financial support from the Netherlands Organization for Scientific Research (NWO, vici grant 724.013.003), the European Research Council (ERC starting grant 280010), the Spanish MINECO (CTQ2017-87889-P), the Ministry of Education, Culture, and Science (Gravitation program no. 024.001.035), a postdoctoral grant from the Xunta de Galicia (I2C Plan, to L.V.), and a PhD grant from the Generalitat de Catalunya (to L.A.C.) are gratefully acknowledged.

Conflict of interest

The authors declare no conflict of interest.

Keywords: artificial metalloenzymes · biocatalysis · carbenes · enzyme design · heme enzymes

How to cite: *Angew. Chem. Int. Ed.* **2018**, *57*, 7785–7789
Angew. Chem. **2018**, *130*, 7911–7915

[1] C. K. Prier, F. H. Arnold, *J. Am. Chem. Soc.* **2015**, *137*, 13992–14006.
[2] O. F. Brandenberg, R. Fasan, F. H. Arnold, *Curr. Opin. Biotechnol.* **2017**, *47*, 102–111.

[3] P. S. Coelho, E. M. Brustad, A. Kannan, F. H. Arnold, *Science* **2013**, *339*, 307 – 310.
[4] P. S. Coelho, Z. J. Wang, M. E. Ener, S. A. Baril, A. Kannan, F. H. Arnold, E. M. Brustad, *Nat. Chem. Biol.* **2013**, *9*, 485 – 487.
[5] M. Bordeaux, V. Tyagi, R. Fasan, *Angew. Chem. Int. Ed.* **2015**, *54*, 1744 – 1748; *Angew. Chem.* **2015**, *127*, 1764 – 1768.
[6] J. G. Gober, A. E. Rydeen, E. J. Gibson-O'Grady, J. B. Leuthaeuser, J. S. Fetrow, E. M. Brustad, *ChemBioChem* **2016**, *17*, 394 – 397.
[7] A. Tinoco, V. Steck, V. Tyagi, R. Fasan, *J. Am. Chem. Soc.* **2017**, *139*, 5293 – 5296.
[8] V. Tyagi, R. Fasan, *Angew. Chem. Int. Ed.* **2016**, *55*, 2512 – 2516; *Angew. Chem.* **2016**, *128*, 2558 – 2562.
[9] M. J. Weissenborn, S. A. Löw, N. Borlinghaus, M. Kuhn, S. Kummer, F. Rami, B. Plietker, B. Hauer, *ChemCatChem* **2016**, *8*, 1636 – 1640.
[10] Z. J. Wang, N. E. Peck, H. Renata, F. H. Arnold, *Chem. Sci.* **2014**, *5*, 598 – 601.
[11] G. Sreenilayam, R. Fasan, *Chem. Commun.* **2015**, *51*, 1532 – 1534.
[12] S. B. J. Kan, R. D. Lewis, K. Chen, F. H. Arnold, *Science* **2016**, *354*, 1048 – 1051.
[13] S. B. J. Kan, X. Huang, Y. Gumulya, K. Chen, F. H. Arnold, *Nature* **2017**, *552*, 132 – 136.
[14] H. M. Key, P. Dydio, D. S. Clark, J. F. Hartwig, *Nature* **2016**, *534*, 534 – 537.
[15] H. M. Key, P. Dydio, Z. Liu, J. Y.-. Rha, A. Nazarenko, V. Seyedkazemi, D. S. Cark, J. F. Hartwig, *ACS Cent. Sci.* **2017**, *3*, 302 – 308.
[16] G. Sreenilayam, E. J. Moore, V. Steck, R. Fasan, *Adv. Synth. Catal.* **2017**, *359*, 2076 – 2089.
[17] K. Oohora, H. Meichin, L. Zhao, M. W. Wolf, A. Nakayama, J. Hasegawa, N. Lehnert, T. Hayashi, *J. Am. Chem. Soc.* **2017**, *139*, 17265 – 17268.
[18] G. Sreenilayam, E. J. Moore, V. Steck, R. Fasan, *ACS Catal.* **2017**, *7*, 7629 – 7633.
[19] T. Yonetani, T. Asakura, *J. Biol. Chem.* **1969**, *244*, 4580 – 4588.
[20] T. Hayashi, H. Dejima, T. Matsuo, H. Sato, D. Murata, Y. Hisaeda, *J. Am. Chem. Soc.* **2002**, *124*, 11226 – 11227.
[21] C. Choma, J. Lear, M. Nelson, P. Dutton, D. Robertson, W. DeGrado, *J. Am. Chem. Soc.* **1994**, *116*, 856 – 865.
[22] C. Reedy, B. Gibney, *Chem. Rev.* **2004**, *104*, 617 – 649.
[23] I. V. Korendovych, A. Senes, Y. H. Kim, J. D. Lear, H. C. Fry, M. J. Therien, J. K. Blasie, F. A. Walker, W. F. DeGrado, *J. Am. Chem. Soc.* **2010**, *132*, 15516 – 15518.
[24] Y. Lin, E. B. Sawyer, J. Wang, *Chem. Asian J.* **2013**, *8*, 2534 – 2544.
[25] C. C. Moser, M. M. Sheehan, N. M. Ennist, G. Kodali, C. Bialas, M. T. Englander, B. M. Discher, P. L. Dutton, *Methods Enzymol.* **2016**, *580*, 365 – 388.
[26] J.-P. Mahy, J.-D. Maréchal, R. Ricoux, *Chem. Commun.* **2015**, *51*, 2476 – 2494.
[27] F. Schwizer, Y. Okamoto, T. Heinisch, Y. Gu, M. M. Pellizzoni, V. Lebrun, R. Reuter, V. Köhler, J. C. Lewis, T. R. Ward, *Chem. Rev.* **2018**, *118*, 142 – 231.
[28] P. K. Madoori, H. Agustiandari, A. J. M. Driessen, A. M. W. H. Thunnissen, *EMBO J.* **2009**, *28*, 156 – 166.
[29] K. Takeuchi, Y. Tokunaga, M. Imai, H. Takahashi, I. Shimada, *Sci. Rep.* **2014**, *4*, 6922.
[30] I. Drienovská, A. Rioz-Martínez, A. Draksharapu, G. Roelfes, *Chem. Sci.* **2015**, *6*, 770 – 776.
[31] J. Bos, A. García-Herraiz, G. Roelfes, *Chem. Sci.* **2013**, *4*, 3578 – 3582.
[32] I. Drienovská, L. Alonso-Cotchico, P. Vidossich, A. Lledos, J. Maréchal, G. Roelfes, *Chem. Sci.* **2017**, *8*, 7228 – 7235.
[33] J. Bos, F. Fusetti, A. J. M. Driessen, G. Roelfes, *Angew. Chem. Int. Ed.* **2012**, *51*, 7472 – 7475; *Angew. Chem.* **2012**, *124*, 7590 – 7593.
[34] J. Bos, W. R. Browne, A. J. M. Driessen, G. Roelfes, *J. Am. Chem. Soc.* **2015**, *137*, 9796 – 9799.
[35] K. A. de Villiers, C. H. Kaschula, T. J. Egan, H. M. Marques, *J. Biol. Inorg. Chem.* **2007**, *12*, 101 – 117.
[36] C. Asher, K. A. de Villiers, T. J. Egan, *Inorg. Chem.* **2009**, *48*, 7994 – 8003.
[37] A. Abu-Elfotoh, K. Phomkeona, K. Shibatomi, S. Iwasa, *Angew. Chem. Int. Ed.* **2010**, *49*, 8439 – 8443; *Angew. Chem.* **2010**, *122*, 8617 – 8621.

Manuscript received: March 9, 2018
Revised manuscript received: May 1, 2018
Accepted manuscript online: May 2, 2018
Version of record online: May 29, 2018

